Progress of Theoretical Physics, Vol. 52, No. 4, October 1974

Molecular Dynamics Studies on the Soft-Core Model

Yasuaki HIWATARI, Hirotsugu MATSUDA,* Tohru OGAWA,**
Naofumi OGITA† and Akira UEDA††

Institute for Spectroscopic Study of Matter, Faculty of Science
Kanazawa University, Kanazawa
**Department of Biology, Faculty of Science*
Kyushu University, Fukuoka
***Department of Physics, Faculty of Science*
Kyoto University, Kyoto
†*Institute of Physical and Chemical Research, Wako, Saitama*
††*Department of Applied Mathematics and Physics*
Faculty of Engineering, Kyoto University, Kyoto

(Received March 22, 1974)

Molecular dynamics studies are made on the soft-core model with a pair potential $\phi(r)=C/r^{12}$, $(C>0)$. Equation of states, self-diffusion constants, velocity autocorrelation functions (v. a. f.) and radial distribution functions (r. d. f.) are computed for a wide range of reduced density $\rho^*=0.05\sim1.9$, where $\rho^*=(N/V)(C/kT)^{1/4}$ and N/V is a number density. $\rho_f^*=1.15$ and $\rho_m^*=1.19$ correspond to the freezing and melting reduced densities, respectively. For $\rho^*\lesssim0.5$, the system is gas-like in a sense that the v. a. f. is not oscillatory and the r. d. f. has only a single peak. For $\rho^*\gtrsim0.5$, the v. a. f. becomes oscillatory and the r. d. f. has more than one peak, in contrast with the hard-core system for which no oscillation of the v. a. f. is observed at all in the fluid phase. In this sense the system behaves like liquid between $\rho^*\simeq0.5$ and 1.15. Around $\rho^*\simeq1.35$, the self-diffusion constant drops abruptly, indicating the limit of supercooling or a kind of glass transition. Comparisons are made with the result of the hard-core system. Diffusion constants of Kr and Lennard-Jones system are found to be well fitted by the soft-core model.

§ 1. Introduction

Since the computer studies of Alder and Wainwright[1] and Wood and Jackobson[2] revealed that even a system of hard spheres may exhibit a solid-fluid phase transition, a great number of works[3] have been carried out on the properties of an assembly of particles interacting with a simple pair potential, using either the molecular dynamics method or the Monte Carlo method. Through the analyses of these works the following has become fairly certain:

(i) A small system containing less than 1000 atoms can represent some of macroscopic properties of the large system very well, so that the computer studies for such a small system will furnish a most reliable data for macroscopic properties of the large model system with the same pair potential.

(ii) There is a part of the pair potential which is rather irrelevant to some prop-

erties of the model system. For instance, the change in the long-range attractive part of the pair potential does not entail any significant change in the pair distribution function.[4]

(iii) Certain model systems with a simple pair potential can be made to represent features of the real substance in nature by giving suitable values for the adjustable parameters of the model.[5] This fact will be related to the statement made in (ii).

Recently, Hoover, Gray and Johnson[6] have published their Monte Carlo results on the thermodynamic properties of the fluid and solid phases for inverse power pair potentials,

$$\phi_n(r) = \varepsilon(\sigma/r)^n, \quad \varepsilon>0, \quad \sigma>0, \quad n>3\,. \tag{1·1}$$

Using their results[6] and the so-called van der Waals theory, Hiwatari and Matsuda[7] have pointed out that the system of particles with a pair potential

$$\phi^{(n)}(r) = \phi_n(r) - \alpha\gamma^3 \exp(-\gamma r), \tag{1·2}$$

is not only simple because of its scaling properties, but also capable of exhibiting three phases of matter. Here, $\alpha(>0)$ is a parameter specifying the strength of the attractive potential and a positive constant γ is a quantity to be made to tend to zero after taking a thermodynamic limit.[8] They have also shown that this model represents various detailed features of the thermodynamic properties of inert gases, alkalies and alkaline earths, whereas those of noble metals and trivalent metals have features which cannot be explained by this model.

In view of these observations it would be worth while making a further systematic investigation of simple models by computer experiments and clarifying the salient relationships between the interatomic potentials and the feature of macroscopic properties of matter. We have started this program by making a molecular dynamics study of the soft-core model with a pair potential $\phi_{12}(r)$, since the attractive part of the potential $\phi^{(12)}(r)$ is irrelevant to dynamical processes occurring inside the system with a fixed density.[9] Although a considerable amount of knowledge has already been accumulated as to the static properties of this soft-core model, only few works have been done on its dynamical properties, so far as the authors are aware.[10] We can obtain rather reliable values for diffusion constants, velocity autocorrelation functions as well as radial distribution functions. From these results we found that the dynamical feature of our model can indeed be classified into three types, gas-like, liquid-like and solid-like, according to the scaled density; the dynamical feature is well correlated with the feature of the pair distribution functions. It is also found that the distinction between gas-like and liquid-like behavior is more pronounced for the soft-core model than for the hard-core model.

In this paper, after recapitulating the scaling properties of the soft-core model in § 2, which is important for our studies, we describe in § 3 the method in

molecular dynamics for the preparation of the states. In § 4 we give the equation of states obtained by our computer experiments and compare it with the result of Hoover et al.[6] In § 5 we give the diffusion constants obtained by our method and compare them with those previously obtained by Ross and Schofield.[10] In §§ 6 and 7 we give the velocity autocorrelation functions and radial distribution functions. Finally, § 8 is devoted to general discussion of our results.

§ 2. Scaling properties of the soft-core model

Suppose that a system of N atoms confined in a cubic box of volume $V=L^3$ has a pair potential given by (1·1). Then, the Lagrangian of the system can be written as

$$\mathcal{L}=\frac{m}{2}\sum_{i=1}^{N}\left(\frac{d\boldsymbol{r}_i}{dt}\right)^2-\sum_{i>j}\sum\phi_n(r_{ij})-\sum_{i=1}^{N}\Omega(\boldsymbol{r}_i), \tag{2·1}$$

where m is a mass of an atom, $r_{ij}=|\boldsymbol{r}_i-\boldsymbol{r}_j|$ and

$$\Omega(\boldsymbol{r})=\begin{cases}0 & \text{if } 0<x,y,z<L, \quad \boldsymbol{r}=(x,y,z),\\ \infty & \text{otherwise,}\end{cases} \tag{2·2}$$

corresponding to the fact that each atom is confined in the cubic box of the side length L.

Now let us introduce the units of length l and time τ, by

$$l=v^{1/3}, \quad \tau=\left(\frac{ml^{n+2}}{C}\right)^{1/2}=l\left(\frac{m}{\varepsilon}\right)^{1/2}\left(\frac{l}{\sigma}\right)^{n/2}, \tag{2·3}$$

respectively, where $C=\varepsilon\sigma^n$ and $v=V/N$ is an atomic volume. Putting

$$\boldsymbol{r}_i=l\boldsymbol{r}_i^*, \quad t=\tau t^* \text{ and } \mathcal{L}=\frac{C}{l^n}\mathcal{L}^*, \tag{2·4}$$

we may rewrite Eq. (2·1) as

$$\mathcal{L}^*=\frac{1}{2}\sum_{i=1}^{N}\left(\frac{d\boldsymbol{r}_i^*}{dt^*}\right)^2-\sum_{i>j}\sum r_{ij}^{*-n}-\sum_{i=1}^{N}\Omega^*(\boldsymbol{r}_i^*), \tag{2·5}$$

where

$$\Omega^*(\boldsymbol{r}^*)=\begin{cases}0 & \text{if } 0<x^*,y^*,z^*<N^{1/3},\\ \infty & \text{otherwise.}\end{cases} \tag{2·6}$$

From Eq. (2·5) we obtain the momentum $\boldsymbol{p}_i^*$ conjugate to $\boldsymbol{r}_i^*$ and the Hamiltonian $\mathcal{H}^*$ of the reduced dynamical system as

$$\boldsymbol{p}_i^*=\frac{\partial\mathcal{L}^*}{\partial(d\boldsymbol{r}_i^*/dt^*)}=\frac{d\boldsymbol{r}_i^*}{dt^*}=\left(\frac{l^n}{Cm}\right)^{1/2}\boldsymbol{p}_i=(\varepsilon m)^{-1/2}(l/\sigma)^{n/2}\boldsymbol{p}_i, \tag{2·7}$$

$$\mathcal{H}^*=\frac{1}{2}\sum_{i=1}^{N}\boldsymbol{p}_i^{*2}+\sum_{i>j}\sum r_{ij}^{*-n}+\sum_{i=1}^{N}\Omega^*(\boldsymbol{r}_i^*)=\frac{l^n}{C}\mathcal{H}, \tag{2·8}$$

where $\boldsymbol{p}_i$ and $\mathcal{H}$ are the momentum of the i-th atom and the Hamiltonian of the original system, respectively. Therefore, so far as the classical mechanics is applicable, we can see the behavior of the original system for all values of atomic volume v from the knowledge of the reduced dynamical system which is independent of v. Note that l, τ and the mass m complete the system of units, and they are independent of whether the system is in equilibrium or not.

When the system is in thermal equilibrium with a heat bath of temperature T, the probability of realization of each state of the system is given by a canonical distribution. Because of the relation (2·8), the canonical distribution of the system with temperature T just corresponds to the canonical distribution $\exp(-\mathcal{H}^*/T^*)$ of the reduced temperature

$$T^* = kT(l^n/C) = \frac{kT}{\varepsilon}\left(\frac{l}{\sigma}\right)^n. \tag{2·9}$$

Therefore the average of any dynamical quantity $f(\boldsymbol{p}, \boldsymbol{r})$ of the original system over the canonical distribution is related to that of the corresponding quantity $f^*(\boldsymbol{p}^*, \boldsymbol{r}^*)$ of the reduced system by

$$\langle f(\boldsymbol{p}, \boldsymbol{r})\rangle_c = l^\alpha \tau^\beta m^\gamma \langle f^*(\boldsymbol{p}^*, \boldsymbol{r}^*)\rangle_{c^*}, \tag{2·10}$$

where

$$\langle f^*(\boldsymbol{p}^*, \boldsymbol{r}^*)\rangle_{c^*} = \int f^*(\boldsymbol{p}^*, \boldsymbol{r}^*) e^{-\mathcal{H}^*/T^*} d\Gamma^* \Big/ \int e^{-\mathcal{H}^*/T^*} d\Gamma^* \tag{2·11}$$

depends on T^* only and α, β and γ are determined by the dimension of $f(\boldsymbol{p}, \boldsymbol{r})$.

Instead of T^*, it is sometimes more convenient to introduce the reduced atomic volume v^* or the reduced density ρ^* defined by

$$v^* = \rho^{*-1} = T^{*3/n} = \left(\frac{kT}{\varepsilon}\right)^{3/n}\left(\frac{l}{\sigma}\right)^3 = \left(\frac{kT}{\varepsilon}\right)^{3/n}\rho^{-1}, \tag{2·12}$$

where $\rho = N\sigma^3/V$, because the equation of state is usually expressed as an isotherm in $P-v(P-\rho)$ plane and $v^*(\rho^*)$ is proportional to $v(\rho)$ for given T. If one knows a reduced quantity as a function of ρ^*, one can obtain the corresponding quantity of the original system at temperature T and atomic volume v satisfying Eq. (2·9) with use of the relation (2·10). For instance, the reduced pressure $P_n^*(\rho^*)$ is related to the original one P by

$$\begin{aligned} P = P_n^*(\rho^*)\,(m/l\tau^2) &= \frac{\varepsilon}{\sigma^3}\left(\frac{kT}{\varepsilon}\right)^{3/n+1}\rho^{*n/3+1}P_n^*(\rho^*) \\ &\equiv \frac{\varepsilon}{\sigma^3}\left(\frac{kT}{\varepsilon}\right)^{3/n+1}\tilde{P}_n(\rho^*), \end{aligned} \tag{2·13}$$

where the last equality defines $\tilde{P}_n(\rho^*)$. The compressibility factor PV/NkT is expressed as

$$PV/NkT = \tilde{P}_n(\rho^*)/\rho^*. \tag{2·14}$$

Similarly the diffusion constant D and the viscosity η can be expressed as

$$D=D_n^*(\rho^*)\,l^2/\tau\equiv\sigma\left(\frac{kT}{m}\right)^{1/2}\left(\frac{\varepsilon}{kT}\right)^{1/n}\tilde{D}_n(\rho^*), \tag{2·15}$$

$$\eta=\eta_n^*(\rho^*)\,(m/l\tau)\equiv\frac{\sqrt{m\varepsilon}}{\sigma^2}\left(\frac{kT}{\varepsilon}\right)^{2/n+1/2}\tilde{\eta}_n(\rho^*), \tag{2·16}$$

respectively, where $D_n^*(\rho^*)$ and $\eta_n^*(\rho^*)$ are the corresponding quantities in the reduced system. $\tilde{D}_n(\rho^*)$ and $\tilde{\eta}_n(\rho^*)$ are defined similarly to $\tilde{P}_n(\rho^*)$. These quantities are the universal functions of ρ^* with n as a parameter. Therefore, the study of our model can be reduced to that of such universal functions.

Finally we note that it is sometimes convenient to introduce the time unit τ_0 by

$$\tau_0=\tau(\varepsilon/kT)^{1/2}(\sigma/l)^{n/2}=l(m/kT)^{1/2} \tag{2·17}$$

for equilibrium states, since for $n=\infty$ τ is not defined uniquely. The universal functions remain unchanged by this transformation.

§ 3. The method of computation and the preparation of states

The method of computation is essentially the same as that of Verlet.[11] First the equations of motion are non-dimensionalized with the following set of units:*) unit length $=\sigma$, unit energy $=\varepsilon$, unit time $\tau'=(m\sigma^2/n\varepsilon)^{1/2}$. Numerical integrations are made with the following difference equations:

$$\begin{aligned}&\boldsymbol{r}_j'(t'+h')=-\boldsymbol{r}_j'(t'-h')+2\boldsymbol{r}_j'(t')+h'^2\sum_k\boldsymbol{F}_{jk}'(t'),\\&\boldsymbol{v}_j'(t')=\frac{1}{2h'}[\boldsymbol{r}_j'(t'+h')-\boldsymbol{r}_j'(t'-h')]\end{aligned} \tag{3·1}$$

for $t'\geqq h'$ and

$$\boldsymbol{r}_j'(h')=h'\boldsymbol{v}_j'(0)+\boldsymbol{r}_j'(0)+\frac{h'^2}{2}\sum_k\boldsymbol{F}_{jk}'(0) \tag{3·2}$$

for $t'=0$. Here $\boldsymbol{r}_j'$ and $\boldsymbol{v}_j'$ are the position and velocity of the j-th atom, respectively, and $\boldsymbol{F}_{jk}'$ is the force from the k-th atom.

In order to prepare fluid and crystalline solid states, the initial phases, that is, a set of $\boldsymbol{r}_j'(0)$ and $\boldsymbol{v}_j'(0)$, are chosen as follows. We distributed atoms in the f.c.c. configuration. For their velocities, first we sample them according to the Maxwell distribution with an initial temperature $T_0'=kT_0/\varepsilon$ and then replace the sampled values by those which are obtained by subtracting the velocity of the center-of-mass system so that the whole system may be at rest. The periodic boundary condition is used and the force range is cut at $r_c=4\sigma$.

*) In what follows, a prime will be attached, for quantities expressed in this system of units, unless otherwise mentioned.

We use the following numerical values for computations: Size of time mesh $h'=1/30$, force range $r_c'=4.0$, initial temperature $T_0'=1.0$, the exponent of the potential $n=12$ and the number of atoms $N=32$ and 108. For $h'=1/30$ the errors in total energies are less than 0.3% for densities with which we are concerned.

After integrating the equation of motion about a hundred time steps, the

Table I. Summarized computed data of density, time steps for integrating the equation of motion, temperature T', compressibility PV/NkT, scaled density and scaled diffusion constant $\tilde{D}_{12}(\rho^*)$ for $N=32$. The group I shows the data obtained from the f.c.c. configuration as an initial state. Data for overheated and crystalline states are also included. Data in the groups II and III are obtained by the compression method and those in the group IV by the cooling method. In the last column, (−5), for example, represents 10^{-5}.

	ρ	time steps	kT/ε	PV/NkT	ρ^*	$\tilde{D}_{12}(\rho^*)$
	0.05	5000	1.07	1.13	0.049	4.41(0) ±2.0(−2)
	0.10	〃	1.04	1.29	0.099	2.14(0) ±2.0(−2)
	〃	3000	1.19	1.28	0.096	1.70(0) ±3.9(−1)
	0.15	〃	1.01	1.47	0.149	1.42(0) ±2.0(−2)
	0.20	〃	1.73	1.64	0.194	9.55(−1) ±1.1(−1)
	〃	〃	0.976	1.73	0.201	9.22(−1) ±2.0(−3)
	0.25	〃	0.944	1.97	0.254	7.08(−1) ±2.6(−2)
	0.30	〃	1.61	2.01	0.266	5.87(−1) ±2.0(−2)
	〃	〃	0.903	2.32	0.308	5.38(−1) ±1.4(−2)
	0.35	〃	0.878	2.58	0.362	4.36(−1) ±1.0(−2)
	0.40	〃	0.749	3.18	0.430	3.51(−1) ±1.3(−2)
	〃	〃	0.830	3.09	0.419	3.82(−1) ±1.1(−2)
	0.45	〃	0.790	3.62	0.477	3.57(−1) ±3.0(−3)
	0.50	〃	0.864	4.09	0.519	2.15(−1) ±4.1(−3)
I	〃	〃	0.744	4.32	0.538	3.09(−1) ±2.4(−2)
	0.55	〃	0.704	5.11	0.600	2.06(−1) ±4.3(−3)
	0.60	〃	0.667	6.02	0.664	1.32(−1) ±6.4(−3)
	〃	〃	0.782	5.56	0.638	1.77(−1) ±6.2(−3)
	0.64	〃	0.574	7.18	0.735	1.16(−1) ±2.9(−3)
	0.65	〃	0.628	7.18	0.730	1.01(−1) ±1.5(−3)
	0.7	2400	0.457	9.67	0.851	7.66(−2) ±1.4(−3)
	0.8	〃	0.383	14.5	1.02	4.25(−2) ±2.3(−3)
	0.85	〃	0.379	16.8	1.08	3.02(−2) ±2.0(−3)
	〃	3000	0.448	15.4	1.039	3.05(−2) ±2.2(−3)
	0.86	〃	0.467	14.9	1.040	3.38(−2) ±6.3(−4)
	〃	〃	melt around the 2200th step.			
	0.9	〃	0.518	14.2	1.06	−4.04(−4) ±2.9(−3)
	1.0	〃	0.521	18.1	1.18	5.36(−5) ±1.7(−3)
	1.14	〃	0.515	26.5	1.35	2.82(−4) ±2.2(−3)
	1.35	〃	0.508	46.5	1.60	

Table I. (continued)

	ρ	time steps	kT/ε	PV/NkT	ρ^*	$\tilde{D}_{12}(\rho^*)$
II	0.90	2000	0.430	18.0	1.12	
	0.96	〃	0.473	20.0	1.16	
	1.02	〃	0.543	21.4	1.19	
	1.08	〃	0.618	23.3	1.22	
	1.15	〃	0.717	25.0	1.25	
	1.22	〃	0.813	27.0	1.29	
	1.30	〃	0.924	29.6	1.33	
	1.38	〃	1.07	31.4	1.36	
	1.47	〃	1.16	36.2	1.41	
	1.56	〃	1.27	41.0	1.47	
	1.66	〃	1.41	45.8	1.52	
	1.76	〃	1.59	51.1	1.57	
	1.87	〃	1.90	53.4	1.59	
	1.99	〃	2.05	62.6	1.66	
III	0.90	5000	0.371	20.1	1.16	2.04(−2) ±1.7(−4)
	1.08	〃	1.01	16.8	1.08	2.55(−2) ±4.2(−4)
	1.22	〃	1.03	22.8	1.21	1.35(−2) ±5.9(−4)
	1.30	〃	0.982	28.2	1.31	9.05(−3) ±9.0(−5)
	1.38	〃	0.908	35.6	1.41	−2.70(−6) ±1.3(−4)
	1.47	〃	1.39	30.9	1.35	1.10(−3) ±1.7(−4)
	〃	〃	1.01	40.0	1.46	7.72(−4) ±6.8(−5)
	1.56	〃	1.05	47.2	1.54	1.53(−5) ±5.9(−5)
	1.66	〃	1.15	54.0	1.60	2.38(−5) ±2.0(−4)
	1.87	〃	1.18	81.0	1.79	−6.10(−6) ±8.0(−5)
IV	0.8	1000	0.184	22.8	1.22	
	〃	〃	0.159	25.8	1.27	
	〃	〃	0.118	32.7	1.36	
	〃	〃	0.0843	42.7	1.48	
	〃	〃	0.0694	50.9	1.56	
	〃	〃	0.0607	57.2	1.61	
	〃	〃	0.0523	65.2	1.67	
	〃	〃	0.0474	71.1	1.71	
	〃	〃	0.0447	75.0	1.74	
	〃	〃	0.0369	86.3	1.83	

total kinetic energy begins to fluctuate around a certain value. Then we assume that the system reaches equilibrium. Therefore, in evaluating various time averages, we use the data after 400 time steps. The temperature kT/ε is evaluated with the formula

$$kT/\varepsilon=\frac{n}{3N}\sum_{k=1}^{N}\overline{v_k'^2}, \tag{3·3}$$

Table II. The same as in Table I, but for $N=108$. Data in the group I are obtained from the f.c.c. configuration as an initial state, those in the group II by the compression method and those in the group III by the cooling method. In the last column, (−5), for example, represents 10^{-5}.

	ρ	time steps	kT/ε	PV/NkT	ρ^*	$\tilde{D}_{12}(\rho^*)$
I	0.3	2000	0.926	2.26	0.306	5.18(−1) ±3.8(−2)
	0.4	〃	0.724	3.22	0.434	3.47(−1) ±2.3(−2)
	0.5	〃	0.757	4.22	0.536	2.65(−1) ±1.8(−2)
	0.6	〃	0.546	6.56	0.698	1.36(−1) ±3.6(−3)
	0.65	〃	0.518	7.76	0.766	1.13(−1) ±1.2(−3)
	0.7	〃	0.614	8.23	0.791	1.12(−1) ±1.8(−3)
	0.8	〃	0.551	11.6	0.929	6.52(−2) ±5.6(−4)
	0.9	〃	0.501	16.3	1.07	3.69(−2) ±1.1(−3)
	0.95	〃	0.572	15.3	1.09	−1.20(−3) ±1.3(−3)
	1.14	〃	0.483	27.9	1.37	−1.08(−4) ±1.1(−3)
	1.35	〃	0.477	49.1	1.62	
II	1.02	2000	0.631	19.1	1.14	2.60(−2) ±5.0(−4)
	1.30	3320	1.05	26.2	1.28	8.08(−3) ±3.0(−4)
	1.76	2000	2.50	31.8	1.40	4.23(−4) ±2.1(−4)
	1.87	1300	2.19	43.2	1.54	2.29(−5) ±1.6(−4)
	1.38	2000	0.699	41.9	1.51	
	1.66	〃	1.024	56.7	1.65	
	1.08	〃	0.400	30.3	1.36	
III	0.85	2000	0.217	24.0	1.25	
	0.85	〃	0.139	32.0	1.39	6.96(−3) ±8.4(−4)
	0.85	〃	0.0675	59.9	1.67	

where $\bar{A}$ denotes such a time average of A.

For the preparation of supercooled fluid and possibly glassy states, an equilibrium state of high-density fluid phase is used as an initial phase and two different methods, that is, rapid cooling and strong compression methods are applied. In the case of the cooling method, first we put all the velocities of the atoms in the initial state equal to zero and integrate the equations of motion for about several ten time steps, until the total kinetic energy becomes of nearly the same order of magnitude as the total potential energy measured from its lowest value, and then make again all the velocities zero. This procedure is repeated until ρ^* reaches a desired range of values and since then the integration has been continued in order to get statistically enough data. In the case of the compression method, the linear dimension of the system together with the relative distances between atoms is reduced instantaneously by a factor of 0.98. The compression method is found to be more effective than the cooling method for generating equilibrium states of larger ρ^*-values. All the runs used by statistical analyses are summarized in Tables I and II for $N=32$ and 108, respectively.

§ 4. The equation of state

According to the classical virial theorem the compressibility factor PV/NkT of our system can be written as

$$\frac{PV}{NkT}=1+\frac{n}{3NT^*}\sum\sum_{i>j}\overline{\left(\frac{1}{r_{ij}^*}\right)^n}. \tag{4·1}$$

The result is summarized in Tables I and II and is shown in Fig. 1, together with the result of a system with 500 atoms obtained by Hoover et al.[6] Even for a system with 32 atoms, our result gives a good agreement with theirs both in fluid and in crystalline phases. The freezing and melting points in Fig. 1 are those determined by Hoover et al.; these values are in our notation

$$\rho_f^*=1.15,\ \left(\frac{PV}{NkT}\right)_f=19.7,\ \rho_m^*=1.19,\ \left(\frac{PV}{NkT}\right)_m=19.0. \tag{4·2}$$

As shown in Fig. 1, the equation of state consists of two separate branches, the amorphous and the crystalline. The crystalline branch exists only for $\rho^*\gtrsim 1.0$, while the amorphous branch extends from $\rho^*=0$ up to the highest density of our experiment.

The states for $\rho^*<\rho_m^*$ on the crystalline branch may be called overheated states. The overheating was observed down to about 20% of the scaled melting density in our experiment. However, this situation may depend on the boundary condition and the system size.

The amorphous branch can be divided into two parts at the density $\rho_g^*=1.30\sim1.35$. All the points of the scaled density less than ρ_g^* lie nearly on a single curve for both cases $N=32$ and 108. Since the reproducibility of the equation of state was good for $\rho^*<\rho_g^*$, the supercooled liquid state with ρ^* such that $\rho_f^*<\rho^*<\rho_g^*$ may indeed be metastable. On the other hand, the points for $N=108$ with the reduced

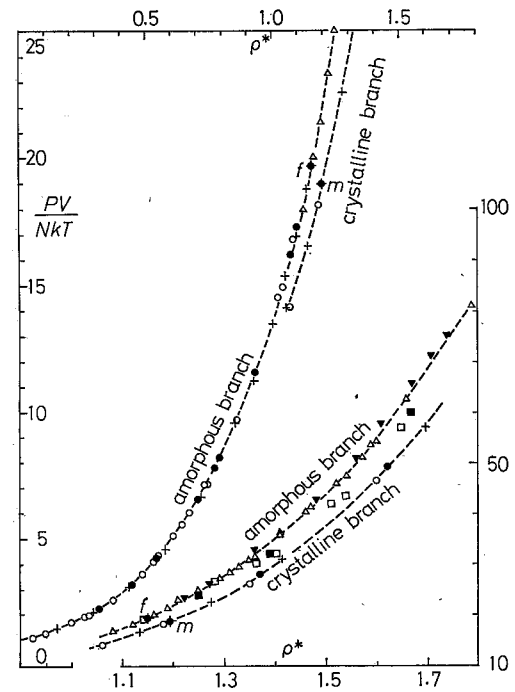

Fig. 1. Equation of state. The plots ○ for $N=32$ and ● for $N=108$ are obtained from the f.c.c. configuration as an initial state. The plots △ and ▼ for $N=32$ are obtained from a high-density fluid state as an initial state by compression and cooling, respectively. The plots □ and ■ for $N=108$ are obtained by compression and cooling, respectively. The crosses + are those obtained by Hoover et al.[6] for $N=500$. The letters f and m indicate the freezing and melting points, respectively.

density larger than ρ_g^* show some deviations from the curve made of points for $N=32$. This deviation also depends on the computing time. Therefore, states with $\rho^*>\rho_g^*$ include non-equilibrium states. From the calculation of the diffusion constant (see § 5), we find that the atomic motion is diffusive for $\rho^*<\rho_g^*$, while it suddenly becomes almost non-diffusive above ρ_g^*. In view of these circumstances, we may associate the thermodynamic point corresponding to $\rho^*=\rho_g^*$ with the so-called glass transition point.

If we keep pressure constant, the ratio of the temperature of the glass transition point to that of the melting point is given from Eqs. (2·13), (2·14) and (4·2) as

$$\frac{T_g}{T_m}=\left[\frac{(PV/NkT)_m\rho_m^*}{(PV/NkT)_g\rho_g^*}\right]^{4/5}=0.63\sim0.66\simeq\frac{2}{3}. \tag{4·3}$$

It is notable that this value is close to the experimental values for most glass-forming substances.[12]

§ 5. Diffusion constant

The diffusion constant not only is an important quantity for the dynamical structure of the system, but also gives a good measure to see whether a simulated system is in the fluid phase or the solid phase, that is, whether the atomic motion is diffusive or non-diffusive.

The diffusion constant is evaluated by three equivalent formulas. The first one is the famous Einstein formula[13]

$$D_n=\lim_{t\to\infty}\frac{1}{6t}\langle R^2(t)\rangle, \tag{5·1}$$

where

$$R^2(t)\equiv\frac{1}{N}\sum_{k=1}^{N}[\boldsymbol{r}_k(t+t_0)-\boldsymbol{r}_k(t_0)]^2$$

is an average over the number of atoms. The position of the k-th particle at time t_0 is designated by $\boldsymbol{r}_k(t_0)$. Even when a particle leaves its original box, its position is traced persistently. The angular bracket represents an ensemble average for which we take a set of initial time t_0 sampled from a long run of a single system after it has reached equilibrium.

The other two formulas are obtained by integrating the velocity autocorrelation function:[14]

$$D_n=\frac{1}{3}\int_0^{t_c}\langle\boldsymbol{v}(t)\cdot\boldsymbol{v}(0)\rangle dt \tag{5·2}$$

with

$$\boldsymbol{v}(t)\cdot\boldsymbol{v}(0)\equiv\frac{1}{N}\sum_{k=1}^{N}\boldsymbol{v}_k(t+t_0)\cdot\boldsymbol{v}_k(t_0),$$

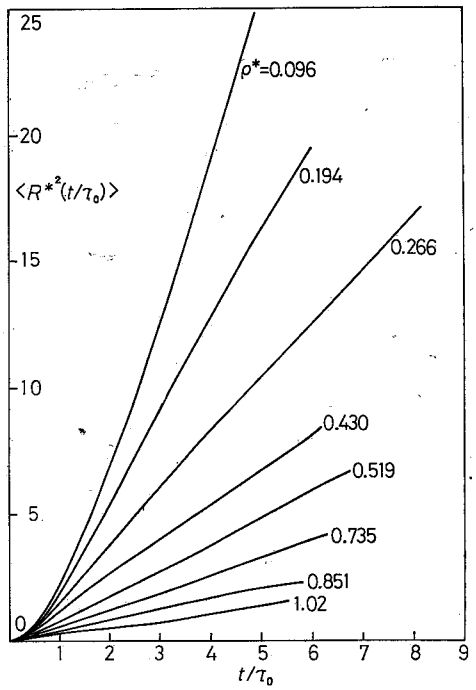

Fig. 2. The mean square displacements of atoms as a function of time t/τ_0 for N=32.

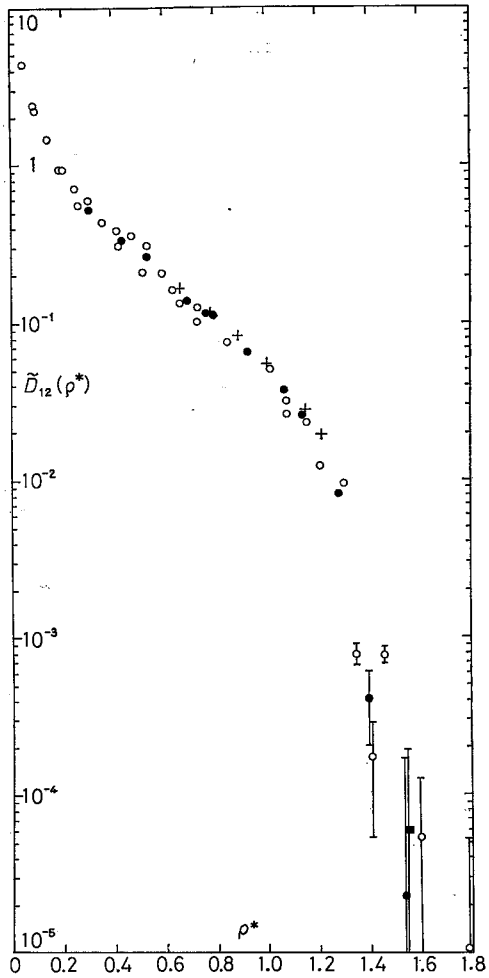

Fig. 3. Diffusion constant for n=12. The plots ○ and ● are for N=32 and 108, respectively. The black square ■ represents the absolute value. The crosses + are those obtained by Ross and Schofield[10] for N=500.

and its integrated form

$$D_n=\frac{1}{3}\langle\{\boldsymbol{R}(t_c)-\boldsymbol{R}(0)\}\cdot\boldsymbol{v}(0)\rangle \tag{5·3}$$

with

$$\{\boldsymbol{R}(t_c)-\boldsymbol{R}(0)\}\cdot\boldsymbol{v}(0)\equiv\frac{1}{N}\sum_{k=1}^{N}\{\boldsymbol{r}_k(t_c+t_0)-\boldsymbol{r}_k(t_0)\}\cdot\boldsymbol{v}_k(t_0).$$

The upper limit of the integral (5·2), t_c, which is limited by the computing time, is taken sufficiently large in connection with the plateau-value problem.

It is found that for higher densities ($\rho^*\gtrsim 0.5$) the formulas (5·2) and (5·3) give smaller and more scattered values than those derived by the formula (5·1).

As will be seen from Fig. 4, for these densities the velocity autocorrelation function has a large negative part which cancels largely the contribution to the integral from the positive part. Beside this, due to statistical errors mentioned in § 5, the integrated value is pretty sensitive to the upper limit of integration. Therefore, in what follows, discussion will exclusively be made on the values obtained by Eq. (5·1).

Figure 2 shows $\langle R^{*2}(t/\tau_0)\rangle$ as a function of t/τ_0 for various densities. From the figure we select the linear parts of the curves and then derive diffusion constants by least square fittings. A particular care is taken for lower densities ($\rho^* \lesssim 0.3$) where a dynamical memory persists longer. For $\rho^* \gtrsim 0.3$, the linearity of the curves is well reproduced for $t \gtrsim 2\tau_0$.

If we denote the diffusion constant expressed in the units of σ, ε and τ' by D_n', $\tilde{D}_n(\rho^*)$ defined by Eq. (2·15) is related to D_n' by the expression

$$\tilde{D}_n(\rho^*) = \sqrt{n}\,(\varepsilon/kT)^{(1/2)-(1/n)} D_n'. \tag{5·4}$$

The evaluated values are summarized in Tables I and II together with the statistical errors. They are plotted as a function of ρ^* in Fig. 3 where the result of Ross and Schofield[10] with $N=500$ is also shown. Though our values are slightly smaller than theirs probably due to the smallness of our system, the general tendency is quite similar.

The ρ^*-dependence of $\tilde{D}_n(\rho^*)$ may be classified into three density regions; low density fluid ($\rho^* \lesssim 0.5$), high density fluid ($\rho^* = 0.5 \sim 1.3$) and still higher densities ($\rho^* > 1.3$). Indeed as can be seen from Fig. 3, there appears an inflection point between the scaled density between $\rho^* = 0.5$ and 0.6, and a rather abrupt drop between $\rho^* = 1.30$ and 1.35. The latter scaled density corresponds to the glass transition point we argued in § 4.

§ 6. Velocity autocorrelation function

The velocity autocorrelation function (v.a.f.) is obtained by the same averaging procedure as that of the diffusion constant. The normalized v.a.f. are plotted as a function of t/τ_0 in Fig. 4. The result for the hard-core system with $N=108$ and 500 by Alder et al.[15] is also plotted. In order to compare their result with ours, the ratio (mean collision time)$/\tau_0 = \sqrt{\pi}/3 \cdot \rho^{1/3}(PV/NkT - 1)^{-1}$ is multiplied to their time.[16]

According to the remark by Zwanzig and Ailawadi,[17] both due to the statistical dependence of the samples and to the limited computing time, relative statistical errors for the normalized v.a.f. become larger with increasing time. For $N=32$ their absolute values are expected to be about 0.02 for the time longer than $\sim 0.7\tau_0$. Probably, small oscillatory features with an amplitude $0.02 \sim 0.03$ which appear for $t \gtrsim 0.6\tau_0$, particularly in the high-density fluid region, will be due to these errors. For $N=108$ the errors are smaller, as it should be. Con-

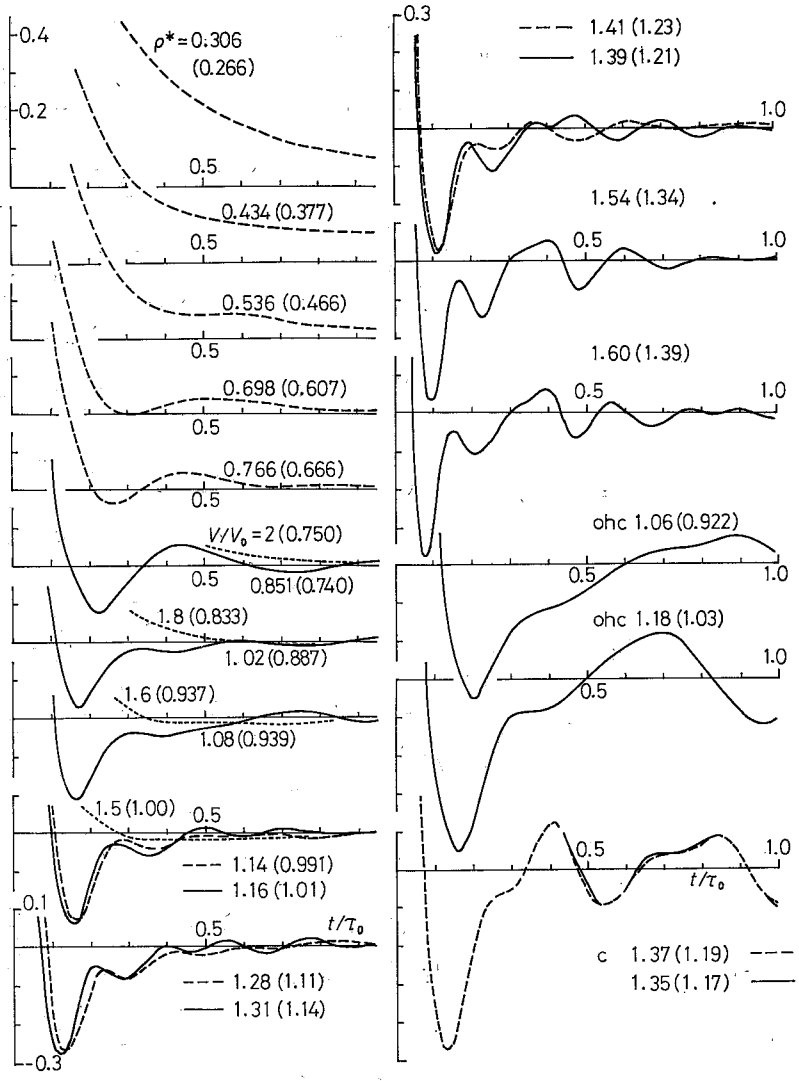

Fig. 4. Velocity autocorrelation function for amorphous, overheated crystalline (ohc) and crystalline (c) states. Solid curves are those for $N=32$ and broken curves for $N=108$. The dotted curves are those for the hard-core system. Figures in the brackets attached to them represent the values of $\bar{\rho}^*$ defined in the text.

sidering these errors and comparing the results of $\rho^*=1.14$ and 1.28 for $N=108$ with respective ones ($\rho^*=1.16$ and 1.31) for $N=32$, we believe that for these high-density region the feature in the time interval before the second maximum is at least qualitatively valid. The characteristic feature so far obtained may be classified into four types, depending on the value of ρ^*. a) For $\rho^* \lesssim 0.5$, the correlation persists for long time with no oscillatory feature. b) Next there ap-

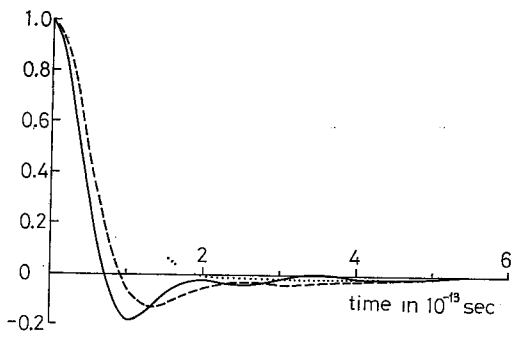

Fig. 5. Comparison of velocity autocorrelation functions.
——: soft-core system for $\rho^*=1.02$ and $\bar{\rho}^*=0.887$.
·····: hard-core system for $V/V_0=1.6$ and $\bar{\rho}^*=0.937$.
– – –: Lennard-Jones system for $\rho=0.84$ and $kT/\varepsilon=0.183$ in our units.

pears a sprout of oscillation for $0.5\lesssim\rho^*\lesssim0.7$ and then c) it grows up at about $\rho^*\simeq0.8$ with a large amplitude. For $\rho^*\lesssim0.7$ the correlation has no negative parts. For $\rho^*\gtrsim0.7$, however, it has negative parts and the first minimum becomes deeper and the first maximum lower with increasing ρ^*, until close to the freezing density. For still higher densities ($\rho^*\simeq1.15\sim1.40$) the correlation has again a wavy feature, but d) above $\rho^*\simeq1.4\sim1.5$, where atoms are practically non-diffusive, it has a somewhat different feature from those of lower densities.

At this moment it is interesting to compare our result with that for the hard-core system.[15] For this system the normalized v.a.f. is obtained in the fluid density region for $V/V_0=3$, 2, 1.8, 1.6 and 1.5, where V_0 is the close packed volume. Setting $n=\infty$ in Eq. (2·12), we find that these values correspond to $\bar{\rho}^*\equiv\rho^*/\rho_f^*=0.500$, 0.750, 0.833, 0.937 and 1.00, respectively. For $\bar{\rho}^*\lesssim0.8$ the v.a.f. has no negative part until it decays nearly to zero. At about $\bar{\rho}^*=0.8$ there appears a negative part and it grows with increasing ρ^*, but its depth is very shallow. The appearance of the negative part at about $\bar{\rho}^*=0.7$ may correspond to that for the soft-core system at about $\bar{\rho}^*=0.7$. This suggests that there occurs some characteristic change in the atomic motion both for the hard-core and the soft-core systems at these densities, respectively. However the change is different from each other. That is, the soft-core system has an oscillatory feature at high-density fluid region, while the hard-core system has none at all over the fluid density region. In Fig. 5 we compare our v.a.f. ($\rho^*=1.02$, $\bar{\rho}^*=0.887$) with those of the hard-core system[15] ($V/V_0=1.6$, $\bar{\rho}^*=0.937$) and of a Lennard-Jones system[4] ($\rho=0.84$, $kT/\varepsilon=0.183$ in our units*)). These states are all near to their respective freezing points. This shows how the softness of the repulsive part of the potentials changes the shape of the v.a.f. particularly around the first minimum.

§ 7. Radial distribution function

The radial distribution function (r.d.f.) is a useful physical quantity for investigating the order of the local structure (short range order) of the state. To

*) Our unit ε corresponds to 4ε in Refs. 4), 21) and 23).

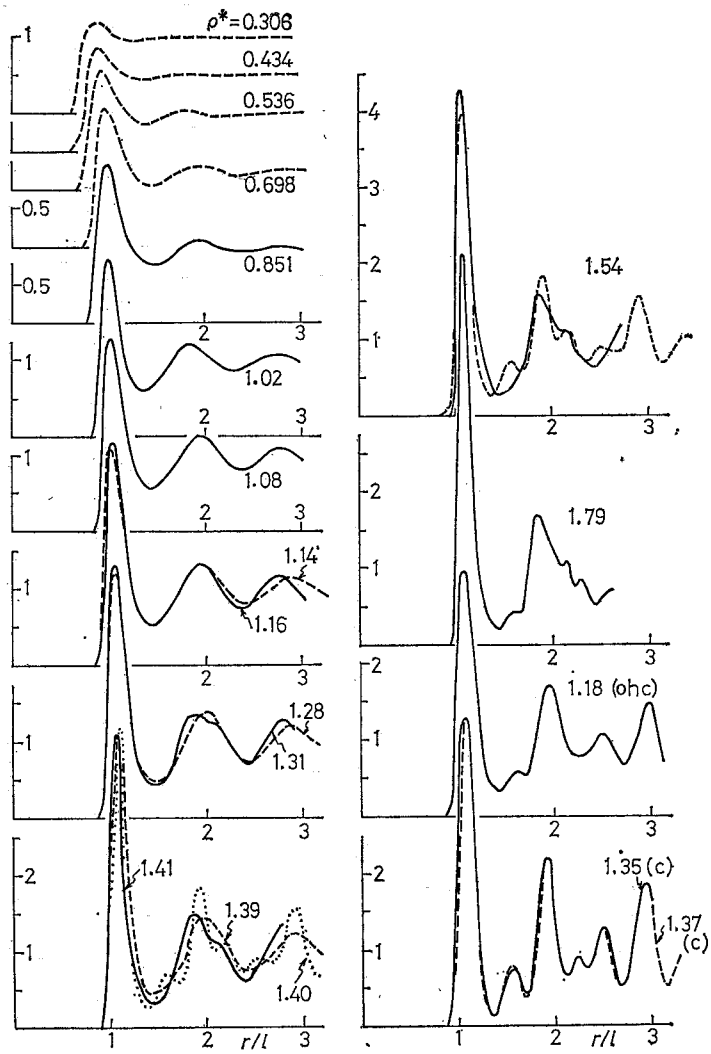

Fig. 6. Radial distribution functions for amorphous, overheated crystalline (ohc) and crystalline (c) phases. The solid curves are those for $N=32$, and broken and dotted curves for $N=108$.

compute the r.d.f. $g(r^*)$, we have used the formula

$$g(r^*)=\frac{\overline{Vn(r)}}{4\pi Nr^2\Delta r}\,, \tag{7·1}$$

where $n(r)$ is the number of atoms situated between r and $r+\Delta r$ from a given atom and r^* is the scaled distance r/l. Then a functional form of $g(r^*)$ becomes a function of only ρ^*. The size of space mesh is $\Delta r^*=0.02$. Our r.d.f. with this mesh reproduces the compressibility factor obtained in § 4 within errors less

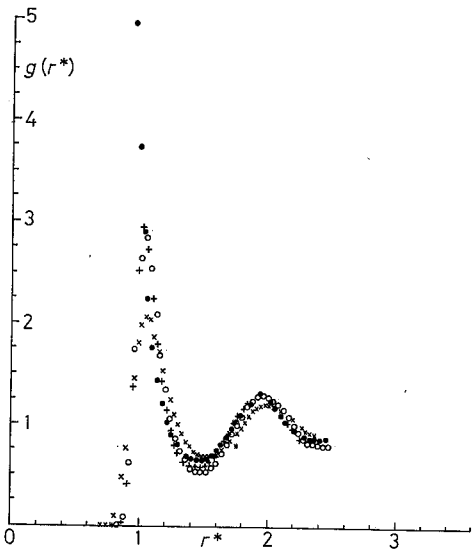

Fig. 7. Comparison of radial distribution functions of the fluid phase close to the melting points.
●: hard-core system for $V/V_0=1.6$ and $\bar{\rho}^*=0.937$.
+: Lennard-Jones system for $\rho=0.850$ and $kT/\varepsilon=0.197$ in our units.
○: soft-core system for $\rho^*=1.16$ and $\bar{\rho}^*=1.01$.
×: Coulomb system for $(4\pi\nu/3)^{1/3}(Ze^2/kT)=100$ where ν is the number of ions with charge Ze per cubic centimenters.

than one percent, when evaluated from the equation[18]

$$\frac{PV}{NkT}=1-\frac{\rho}{6kT}\times\int r\frac{d\phi_n(r)}{dr}g(r)dr\,. \tag{7·2}$$

Figure 6 shows the r.d.f. for various densities. At low density ($\rho^*\lesssim 0.5$) only one peak is observed, at intermediate densities ($0.5\lesssim\rho^*\lesssim 0.8$) the second peak appears and at high densities ($0.8\lesssim\rho^*\lesssim 1.3$) the third peak appears. All these peaks are situated in the region $r^*<3$. The r.d.f. obtained for the amorphous states of $\rho^*>\rho_g^*$, depends on the system size as in the case of the equation of state. There the r.d.f. for $N=108$ has a fine structure similar to that of crystalline state.

Lastly we make a comparison of our r.d.f. with those of hard-core,[19] Coulomb[20] and the Lennard-Jones potentials[21] in Fig. 7. The first peak is very high in the case of hard-core potential, and its height decreases as the softness of a potential increases. This result reconfirms Schiff's conclusion[4),22)] that the height of the second and third peaks of the structure factor $S(Q)$ decreases more rapidly for a system with a potential of softer repulsive part.

§ 8. Discussion

From the static point of view, the distinction between gas and liquid can be made only when both phases are in coexistence; no intrinsic notion of liquid and gas can be attached to the one-phase fluid, not to say that no distinction can be made when the temperature is above the critical point. Even the distinction of fluid and solid should rely on the internal symmetry of the atomic structure. On the other hand, from the dynamical point of view, our study on the soft-core model with $n=12$ indicates that the state of the system can naturally be classified into gas-like, liquid-like and solid-like phases.

Table III. Classification of characteristic features in diffusion constant (d.c.), velocity autocorrelation function (v.a.f.) and radial distribution function (r.d.f.) according to the scaled density ρ^*.

ρ^*	0.2 – 0.4	0.6 – 0.8	1.0 – 1.2	1.4 – 1.6 – 1.8 – 2.0
d.c.	gas-like	liquid-like		non-diffusive
v.a.c.	non-oscillatory	sprout of oscillation	oscillatory	oscillatory (amorphous) oscillatory (crystal)
r.d.f.	1st peak	1st, 2nd peaks	1st, 2nd, 3rd peaks	fine structure

In the gas-like state ($\rho^* \lesssim 0.5$), the velocity autocorrelation function is non-oscillatory and the radial distribution function has only a single peak. We remember that in Fig. 4 there is an inflection point of $\ln D_n(\rho^*)$ at about $\rho^* \simeq 0.5$.

In the region $0.5 \lesssim \rho^* \lesssim 1.3$, the system can be a fluid in the sense that the self-diffusion constant has no discontinuous drop from the gas-like state. However, this region distinguishes itself from the gas-like state in that the v.a.f. is oscillatory and the r.d.f. has more than one peak, showing a considerable correlation of motion between atoms. Hence we may regard this region as a liquid-like state. Since the freezing point is given by $\rho^* = \rho_f^* = 1.15$, the liquid-like region $1.15 \lesssim \rho^* \lesssim 1.3$ correspond to the supercooled liquid. It is to be noted that a dynamical distinction between the gas-like and the liquid-like is not so conspicuous in the hard-core system, where no oscillation is observed in the v.a.f. at any density in the fluid phase.

We may further sub-divide the liquid-like region at $\rho^* \simeq 0.7$. Namely, in the liquid-like state for $\rho^* < 0.7$, the v.a.f. has no negative part and its oscillation is rather weak, but for $\rho^* > 0.7$ a large negative part and strong oscillation are observed. Also the third peak of the r.d.f. is observed only for $\rho^* > 0.7$. These features are summarized in Table III.

At the scaled density $\rho^* = \rho_g^* = 1.3$ there occurs an abrupt drop in the diffusion constant; beyond this scaled density the system practically loses its fluidity, so that the state is solid-like. This solid-like state is not necessarily crystalline but can be amorphous. However, whether the amorphous solid persists for long time when N is sufficiently large needs further scrutiny. The melting point is given by $\rho^* = \rho_m^* = 1.19$,[6] but the solid-like state starting from the crystalline solid state, persists up to the lowest density $\rho^* \simeq 1.0$ in our molecular dynamics studies; this value is considerably lower than ρ_m^*. This phenomenon of overheating will probably be due to the periodic boundary condition. It is not yet certain whether the crystalline solid without a free surface should show such a strong overheating.

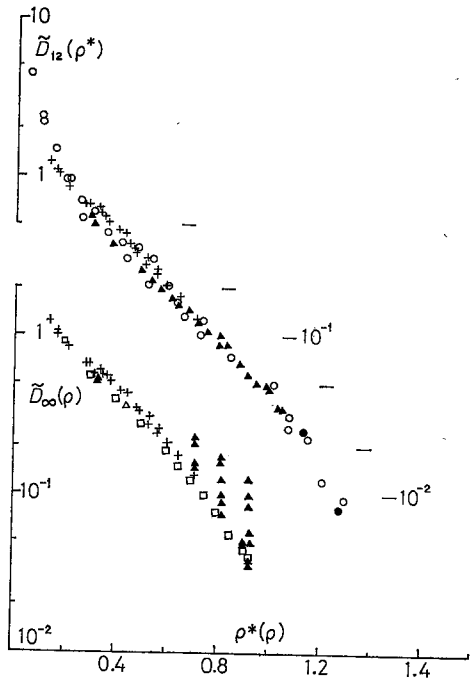

Fig. 8. Comparion of diffusion constants of hard- and soft-core systems with experiments. The ordinate is $\tilde{D}_n(\rho^*)$ for $n=12$ and ∞, or the experimental values evaluated by the procedure described in the text.
○, ●: soft-core system with $N=32$ and 108, respectively.
□: hard-core system.
▲: Lennard-Jones system simultated by a molecular dynamics method.
+: experiment for Kr.

Previously it was shown that the thermodynamic behavior of many real simple liquids can more adequately be fitted by the soft-core model than the hard-core model. In order to see such a correspondence with the real system for the self-diffusion constant, we determine the parameter $\varepsilon^{1/n}\sigma$ by the relation $\rho_t^* = n_t\sigma^3(\varepsilon/kT_t)^{3/n}$, where n_t is the number density of the solid phase and T_t is the temperature at the triple point. In this relation we approximate ρ_t^* by ρ_m^*, which is about 1.19 for $n=12$ and 1.04 for $n=\infty$. Then, invoking Eq. (2·15), we can evaluate $D_n(\rho^*)$ from the experimental data of real substances. If the diffusion constant of the real substance could indeed be well represented by our model, the evaluated $D_n(\rho^*)$ should be a function of only ρ^* and should be close to that obtained by the molecular dynamics method.

As such experimental data we have taken those for Kr by Carelli, Modena and Ricci[28] and those for a Lennard-Jones system by the molecular dynamics studies of Levesque and Verlet.[24] Comparisons with the hard- and soft-core systems are made separately as shown in Fig. 8. For Kr data, both the models give an agreement of the same extent with the experiment. This is because the experiment was done only for a narrow temperature range 180~230°K and only at a normal pressure. On the other hand, the Lennard-Jones system was simulated at temperatures ranging by a factor of more than 5 and also for various densities, so that we can clearly see the difference of fitness between the two models. The soft-core model gives a good agreement with the Lennard-Jones system which is supposed to be good enough for representing Kr.

Thus, we may conclude that the substantial improvement can be gained by the soft-core model over the hard-core model for representing both the dynamical and static features of real substances without impairing the mathematical simplicity. We hope our result may also be of help for interpolating or extrapolating the behavior of real substances under various conditions; especially at high

temperature and/or at high pressure where the experimental approach is not easy.

Acknowledgements

The authors express their thanks to Miss Y. Nakagawa for her assistance. Numerical computations were carried out on the computers of Data Processing Center, Kyoto University and of the Institute of Physical and Chemical Research. This work is financially supported by the Research Institute for Fundamental Physics, Kyoto University, as a research project.

References

1) B. J. Alder and T. E. Wainwright, J. Chem. Phys. **27** (1957), 1208.
2) W. W. Wood and J. D. Jacobson, J. Chem. Phys. **27** (1957), 1207.
3) H. N. V. Temperley, J. S. Rowlinson and G. S. Rushbrooke, edited, ***Physics of Simple Liquids*** (North-Holland, Amsterdam, 1968), Chapts. 4 and 5, and the references cited therein.
4) D. Schiff, Phys. Rev. **186** (1969), 151.
5) H. C. Longuet-Higgins and B. Widom, Mol. Phys. **8** (1964), 549.
N. W. Ashcroft and J. Lekner, Phys. Rev. **145** (1966), 83.
D. Levesque and L. Verlet, Phys. Rev. A **2** (1970), 2514 and the references cited therein.
6) W. G. Hoover, S. G. Gray and K. W. Johnson, J. Chem. Phys. **55** (1971), 1128.
7) Y. Hiwatari and H. Matsuda, Prog. Theor. Phys. **47** (1972), 741.
8) J. L. Lebowitz and O. Penrose, J. Math. Phys. **7** (1966), 98.
9) P. Résibois, J. Piasecki and Y. Pomeau, Phys. Rev. Letters **28** (1972), 882.
10) M. Ross and P. Schofield, J. Phys. C **4** (1971), L305.
11) L. Verlet, Phys. Rev. **159** (1967), 98.
12) S. Sakka and J. D. Mackenzie, J. Non-Crys. Solids **6** (1971), 145.
S. Seki, Chemistry and Engineering **23** (1970), 52 (in Japanese).
13) A. Einstein, Ann. de Phys. **17** (1905), 549.
E. Helfand, Phys. Rev. **119** (1960), 1.
D. M. Gass, J. Chem. Phys. **51** (1968), 4560.
14) P. A. Egelstaff, ***An Introduction to the Liquid State*** (Academic Press, London and New York, 1967) Chapt. 11.
15) B. J. Alder, D. M. Gass and T. E. Wainwright, J. Chem. Phys. **53** (1970), 3813.
16) T. E. Wainwright and B. J. Alder, Nuovo Cim. Suppl. **9** (1958), 116.
17) R. Zwanzig and N. K. Ailawadi, Phys. Rev. **182** (1969), 280.
18) P. A. Egelstaff, ***An Introduction to the Liquid State*** (Academic Press, London and New York, 1967) Chapt. 7.
19) B. J. Alder and C. E. Hecht, J. Chem. Phys. **50** (1969), 2032.
20) S. G. Brush, H. L. Sahlin and E. Teller, J. Chem. Phys. **45** (1966), 2102.
21) L. Verlet, Phys. Rev. **165** (1968), 201.
22) D. Schiff, ***The Properties of Liquid Metals*** ed. by S. Takeuchi (Taylor and Francis, London, 1973), p. 57.
23) P. Carelli, I. Modena and F. P. Ricci, Phys. Rev. A **7** (1973), 298.
24) D. Levesque and L. Verlet, Phys. Rev. A **2** (1970), 2514.